Functionalizing Carbon Nanotubes with Bis(2,9-dialkyl-1,10-phenanthroline)copper(II) Complexes for the Oxygen Reduction Reaction

Deborah Brazzolotto, Yannig Nédellec, Christian Philouze, Michael Holzinger, Fabrice Thomas, Alan Le Goff

Functionalizing carbon nanotubes with bis(2,9-dialkyl-1,10-phenanthroline)copper(II) complexes for Oxygen Reduction Reaction

Deborah Brazzolotto, [a] Yannig Nédellec, [a] Christian Philouze,[a] Michael Holzinger, [a] Fabrice Thomas[a] and Alan Le Goff[a]*

[a] Univ. Grenoble Alpes, CNRS, DCM, 38000 Grenoble, France

E-mail: alan.le-goff@univ-grenoble-alpes.fr

Functionalizing carbon nanotubes with bis(2,9-dialkyl-1,10-phenanthroline)copper(II) complexes for Oxygen Reduction Reaction

Deborah Brazzolotto, [a] Yannig Nédellec, [a] Christian Philouze,[a] Michael Holzinger, [a] Fabrice Thomas[a] and Alan Le Goff[a]*

[a] Univ. Grenoble Alpes, CNRS, DCM, 38000 Grenoble, France

E-mail: alan.le-goff@univ-grenoble-alpes.fr

KEYWORDS copper complexes, oxygen reduction, carbon nanotubes, bioinspired catalysts, fuel cells

ABSTRACT A new ligand 2-(5-(pyren-1-yl)pentyl)-9-methyl-1,10-phenanthroline was designed to form novel bis(2,9-dialkyl-1,10-phenanthroline)copper(II) complexes which were then immobilized on multi-walled carbon nanotube (MWCNT) electrodes. These complexes show a high tendency of auto-reduction into their copper(I) form according to electrochemical and EPR experiments. While these complexes exhibit strong interactions with MWCNT sidewalls either with or without anchor functions like the pyrene moiety. However, the pyrene-based complexes can be electropolymerized on glassy carbon and MWCNT electrode to form a poly-[bis(2-(5-(pyren-1-yl)pentyl)-9-methyl-1,10-phenanthroline)copper(II)] metallopolymer film. Furthermore,

this MWCNT-supported bis(2,9-dialkyl-1,10-phenanthroline)copper complexes demonstrate low overpotential for $4H^+/4e^-$ Oxygen Reduction Reaction at pH 5 with an onset potential of 0.91 V vs. RHE. Integration of these functionalized MWCNTs at gas-diffusion electrodes of H_2/air fuel cells led to a high open-circuit voltage of 0.84 V and a maximum current density of 1.77 mW cm^{-2} using a Pt/C anode.

Introduction

Dioxygen activation is not only a fundamental step in biological processes, but is also at the heart of the generation of electricity in fuel cells or metal-air batteries. .[1–3]. Conventional fuel cells need precious metals or alloys to perform long-term electrocatalytic oxidation of the fuel as well as reduction of the oxidant, oxygen in most cases. [1,2] One encouraging alternative is the use of oxygen-reducing enzymes within enzymatic fuel cells. [4–7] Purified redox enzymes replace metal catalysts, promoting the electrocatalytic reactions. Several copper-containing oxidoreductases are great catalysts towards the $4H^+/4e^-$ Oxygen Reduction Reaction (ORR) providing low overpotentials, high substrate specificity and high catalytic turnover frequency at low temperature and atmospheric pressure. [8–11] Besides, these biomacromolecules are composed of organic amino acids surrounding cofactors made of base-metal active sites. Nevertheless, there are drawbacks using these enzymes. Complicated to handle and to purify, these biocatalysts can also be considered as big catalysts when compared to metal atoms or molecular complexes. Furthermore, intrinsic stability of enzymes is not compatible with many industrial processes. This is why molecular chemists and electrochemists have imagined the use of molecular catalysts, inspired from the enzymatic mechanism and the structure of the active site to execute electrocatalytic reactions. [3,12–24]

The majority of bio-inspired molecular complexes for O_2 reduction has mostly been inspired from heme and copper enzymes. While heme-based enzymes are mostly involved in low-and mid-potential reduction of O_2, multicopper oxidases such as laccases [8–10] have shown efficient electrocatalytic performance towards oxygen reduction reactions (ORR). [4–6,11] During the last decades, bio-inspired copper catalysts have been developed to reproduce the enzymatic activity in order to be integrated into conventional fuel cell systems. [3,12–22]. While important breakthroughs have been made towards molecular catalysts for low-overpotential bioinspired hydrogen oxidation,[23,25–30] there is still no copper complexes possessing low-overpotential ORR, approaching performances of laccases, Pt catalysts or pyrolized M-N-C catalysts.[31,32] We and other have particularly developed the design of copper complexes with trispyridinemethylamine, [33,34] hexaazamacrocycle,[35] triazole, [36,37] polyimidazole, [38] or phenolate ligands.[39–41] However, the best performances have mostly been obtained in alkaline media with maximum ORR onset potentials of around 1 V vs. RHE at pH 13.[36,38,42] Below neutral pH, best results have been obtained for dinuclear copper complexes based on different trispyridylmethylamine [33,40,41] and triazol[36,43,44] ligands with onset potentials of 0.82 V vs. RHE at pH 7.

Carbon nanotubes (CNTs) have demonstrated their great ability to behave as a quasi-ideal support material for these molecular catalysts. CNTs have high conductivity both in terms of ballistic transport and as nanostructured layer. Their three-dimensional nanostructured architecture affords the optimization of molecular catalyst loadings. In addition, we and other have taken benefits of their pi-extended sidewall network to firmly immobilize metal complexes either with pi-extended ligands such as porphyrins[45,46] or by introducing pyrene moiety in the structure of ligands such as polypyridinyl, [47–51], cyclam,[52] bisphosphine[53], cyclopentadienyl[54] or n-

heterocyclic carbenes.[55] This use of CNTs as a molecular catalyst support have also been highly efficient in the integration of molecular catalysts in functional devices such as fuel cells.[25,27,28,40]

In the field of copper complexes for bioinspired ORR, Chidsey et al.[56] used a series of phenanthroline-based ligands adsorbed on Edge Pyrolytic Graphite (EPG) electrodes. Ligands were drop-casted on EPG electrodes followed by soaking the electrodes in the presence of $Cu(NO_3)_2(aq)$ to form the corresponding monophenanthroline complexes on the electrode surface. They specifically studied how the electrocatalysis rate as the redox potential increases due to the modification of the groups attached in particular position of the phenanthroline ring. The E^0_{cat} of Cu complexes of phenanthroline -based ligands is more positive with electron-withdrawing groups on the ligand, while several ligands also increase the steric demands near the Cu center by adding different groups to the 2 and 9 positions on the phenanthroline. More recently, R. Venegas and colleagues[57] further investigated a series of bis(1,10-phenanthroline)copper(I) complexes modified with electron withdrawing or electron pushing methyl groups at the 2 and 9 positions of the ligand. As already observed before, they demonstrated that steric constraints brought by bulky groups at the 2 and 9 positions are prominent as compared to electron withdrawing in the increase of the redox potentials of the Cu(II)/Cu(I) couple[58,59] involved in the ORR activity of these complexes. This is caused by the change in the energy needed to operate the interconversion between the more favorable Cu(I) pseudo tetrahedral conformation and the Cu(II) square planar conformation.

At the light of these results and in order to progress toward the synthesis of copper-based ORR catalysts with minimal ORR overpotential requirement at low to medium pHs, we synthesized a series of bis(2,9-dialkyl-1,10-phenanthroline)copper(II) catalysts where the positions 2 and 9 were modified with ethyl, n-Butyl, and a 1-pyrenylpentane groups. Their adsorption on MWCNT

electrodes and ORR performances were studied followed by their integration and evaluation in a hydrogen/air fuel cell.

Results and Discussion

1. Synthesis and characterization of copper(II) complexes

The ligand 2-(5-(pyren-1-yl)pentyl)-9-methyl-1,10-phenanthroline was obtained from the addition of 1-(4-bromobutyl)pyrene (1eq.) to a solution of neocuproine (1 eq.) and lithium diisopropylamine (1eq.) under argon at -78°C in anhydrous THF in a yield of 37% (figure 1A). The monofunctionalized derivative is the main product of the reaction and was characterized by mass spectrometry and ^{1}HNMR (see ESI for details). The different bis(2,9-dialkyl-1,10-phenanthroline)copper(II) complexes were formed by adding a methanol solution of $Cu(ClO_4)_2.6H_2O$ to a solution of the corresponding ligand in MeCN (Figure 1B). Each complex was isolated in the solid state by precipitation in Et_2O and subsequent drying under vacuum. Mass spectroscopy confirms the isolation of the bis-phenanthroline derivative for all complexes.

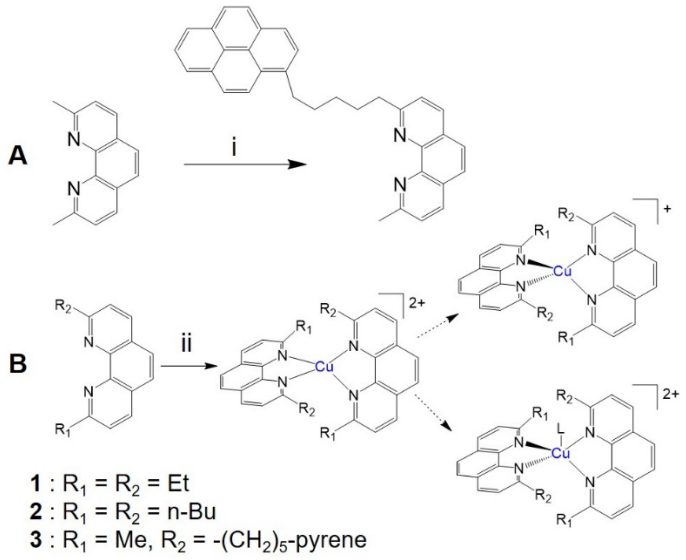

Figure 1. (A) Simplified synthetic procedure leading to 2-(5-(pyren-1-yl)pentyl)-9-methyl-1,10-phenanthroline and (B) complexes **1**, **2** and **3** respectively. (i) 1-(4-bromobutyl)pyrene; (ii) $Cu(ClO_4)_2.6H_2O$.

Perchlorate anion was chosen for its weakly-coordinating property. As it was already observed for the 2,9-dimethyl-1,10-phenanthroline (dmp) ligand, this type of copper complex is prone to extend their coordination sphere by accommodating a fifth ligand such as chloride or MeCN when the metal ion lies under its (+II) oxidation state (Figure 1B).[60,61] This is the reason why complex **1** was crystallized in its Cu(II) form with a water molecule as a coligand. Note that only the Cu(I) form has been previously characterized .[62] The X-ray structure of **1** is depicted in Fig. 2 and the selected bond lengths and angles are reported in table 1. Complex **1** crystallizes from the corresponding Cu(II) powder as disordered Cu complex. According to the crystallographic data, 70% of the structure appears to be a five-coordinate molecule with the coordination of a water molecule in the axial position with a Cu---O of 2.101(5) Å and 30% without. In the main structure, the Cu is described as a distorted trigonal-bipyramidal geometry with a τ_5 = 0.93, which is consistent with a four-coordinated structure around the Cu presenting a distorted trigonal pyramidal geometry. Interestingly, in the case of complex **2**, all attempts to crystallize the copper(II) form of the complex lead to the copper(I) counterpart, as demonstrated by a yellow shade instead of a pale blue color. Complex **2** was thus isolated as single crystals and subsequent X-ray diffraction analysis confirmed its Cu(I) oxidation state. The obtained structure is consistent with the previously reported one which was obtained using a Cu(I) precursor. [63] Attempts to crystallize complex **3,** either in its Cu(I) or Cu(II) form were unsuccessful, likely due to the flexibility of the pyrene linkers.

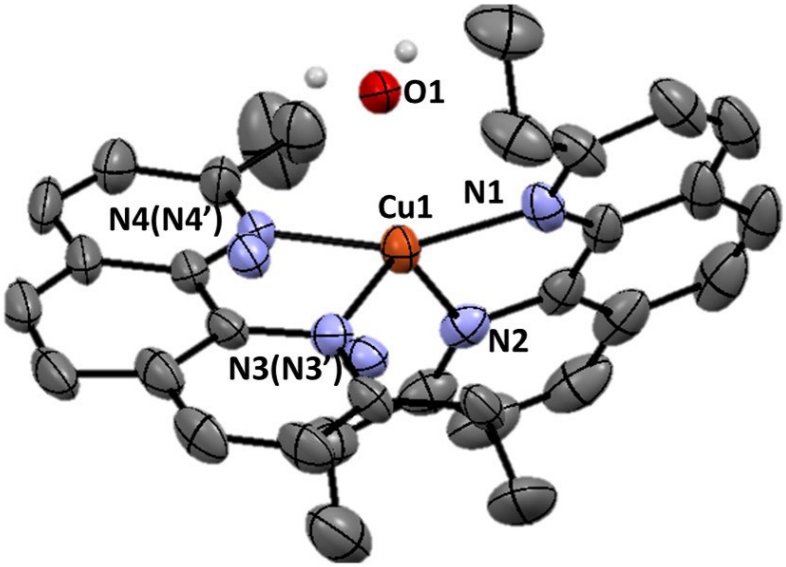

Fig. 2 ORTEP-type views of **1** (thermal ellipsoids set at 30% probability, hydrogen atoms and ClO_4^- anion are removed for more clarity).

Table 1: Selected bond length (Å) and angles (°) for complex **1**.

	Complex 1
Cu-N1	1.987(4)
Cu-N2	2.088(5)
Cu-N3	2.02(2)/2.184(9)
Cu-N4	2.03(2) /2.007(9)
Cu-O1	2.101(5)
N1-Cu-N3	154.9(6)
1N2-Cu-N4	116.7(10)
N1-Cu-N2	82.20(2)
N3-Cu-N4	83.20(7)
N1-Cu-N4	118.4(7)
N2-Cu-N3	100.1(8)

Electrochemistry and EPR characterization in organic solvents

The tendency of these series of Cu(II) complexes to be easily reduced into their Cu(I) form (Figure 1B) was investigated by electrochemistry and EPR experiments, either in DMF or in MeCN. When cyclic voltammetry of a fresh Cu(II) complex solution is performed in a coordinating solvent such as MeCN, the expected reversible system corresponding to the Cu(I)/Cu(II) redox couple is observed at $E_{1/2}^{red}$ = 0.43 and 0.45 V vs. Fc/Fc^+ for complex **1** and **2** respectively (Figure 3).

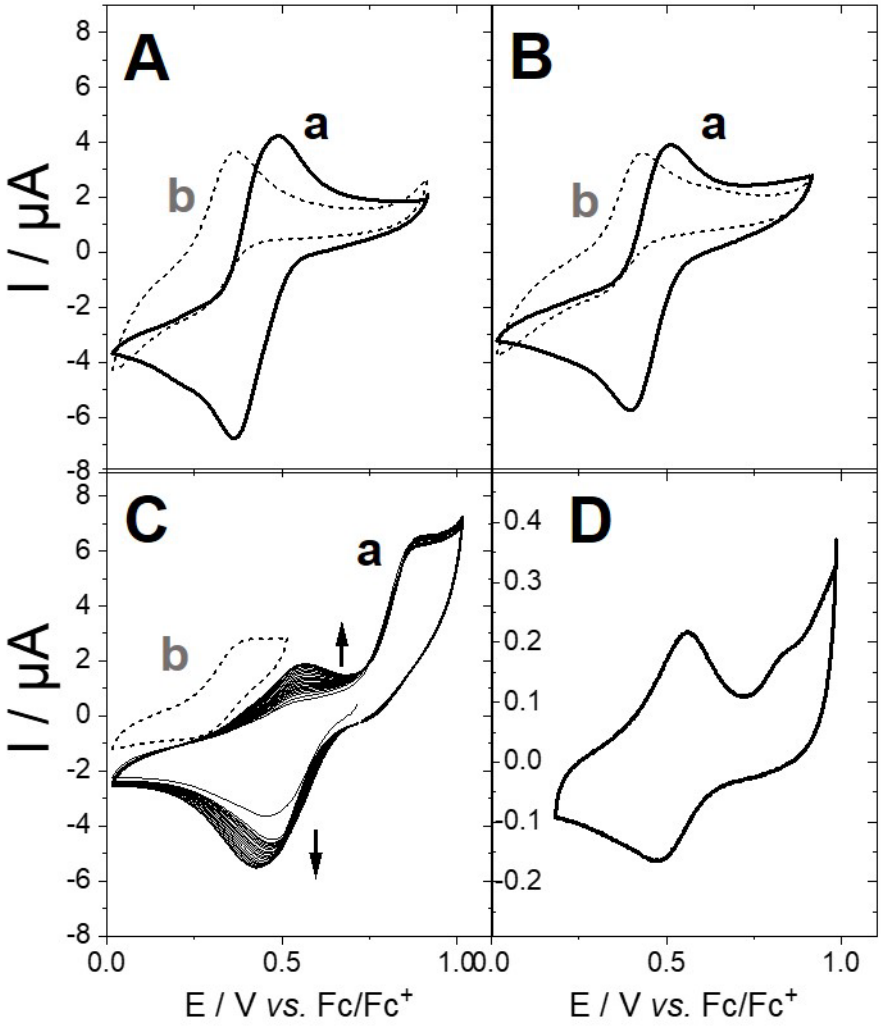

Figure 3. CVs of a solution of complex (A) **1**, (B) **2** and (C) **3** (20 scans) in 0.1 mol L^{-1} MeCN-TBAP (a) before and (b) after addition of 10 % DMF (v = 100 mV s^{-1}) ; (D) CV of a GC electrode

modified by electropolymerization of complex **3** in a 0.1 mmolL^{-1} solution by 20 CV scans between 0 and 1.1 V (0.1 molL^{-1} MeCN-TBAP (v = 10 mV s^{-1})

The redox system matches the redox potential measured for the previously-characterized Cu(I) form of these complexes.[62,64] A shift towards more positive values for these series of complexes as compared to the parent complex bearing the dmp ligand[60] is expected from the distortion of the favored square-pyramidal geometry of the Cu(II) form over a tetrahedral geometry for the Cu(I) form. For complex **3**, this redox system observed at $E_{1/2}$ = +0.48 V vs. Fc/Fc^+ is less reversible. Furthermore, an irreversible oxidation is observed at E_p^{ox} = 0.89 V vs. Fc/Fc^+ and corresponds to the oxidation of the pyrene groups. As already observed for bipyridine complexes bearing pyrene moiety,[49,55] this oxidation lead to the electropolymerization of pyrene and the subsequent electrodeposition of complex **3** at the surface of the GC electrode. This is assessed by the increase of the $Cu^{II/I}$ redox system upon successive scans above the oxidation of pyrene (Figure 3C). After transferring the electrode in a complex-free solution, CV confirms the attachment of complex **3**, thanks to the formation of the electrogenerated poly-(pyrene)-based metallopolymer film. The reversible system is typical of a surface-confined redox process with linear dependence of both anodic and cathodic peaks towards scan rate. According to the integration of the charge under the redox peaks, a surface coverage of 4.6 pmol cm^{-2} was estimated.

Diffusion-controlled linear sweep voltammetry was used to monitor the evolution of the complex in solution (Figure S2). After 2 hours, the slow reduction of the complex in its Cu(I) state is observed by the appearance of an oxidation current corresponding to the formation of the Cu(I) specie in solution. A distribution of 15% Cu(I) and 85% Cu(II) can be estimated from the LSV experiment. Furthermore, if a non-coordinating solvent such as DMF is added to the electrolyte, a

rapid full reduction of each complex into their Cu(I) form is observed. This is confirmed by CV and LSV performed after addition of DMF (curves b from figure 2A-C and curve c from figure S2A-C).

This fast reduction of the Cu(II) form was also monitored by EPR spectroscopy both in DMF and CH_3CN (figure 4, figure S3). The Cu(II) species were generated *in situ* from the ligand and a copper(II) salt and quickly transferred into the EPR cavity for analysis. A blank against $Cu(ClO_4)_2$ 6 H_2O confirmed the initial formation of the Cu(II) form for all the complexes in CH_3CN. For **1** and **2** the intensity of the copper lines decayed to about two thirds of the initial signal after 3h30 at room temperature and one half after one day, confirming Cu(II) reduction. Complex **3** was found to be more robust towards reduction, with only 10% decrease after one day and 50% after 10 days. The spin Hamiltonian parameters were determined by spectral simulation: They are $g_{\perp} = 2.080$, $g_{//} = 2.275$, with $A_{\perp} = 50$ and $A_{//} = 410$ MHz (for the copper nucleus) for the three complexes. This similarity is in line with the expected identical coordination sphere in **1**, **2** and **3**. When the same experiment was conducted in DMF the signal intensity was already less than 20% after 10 sec mixing (Fig S3 and S4). The residual signal was fitted with spin Hamitlonian parameters that correspond to free copper ($g_{\perp} = 2.081$, $g_{//} = 2.403$, with $A_{\perp} = 20$ and $A_{//} = 405$ MHz), suggesting that the copper ion chelated to the ligand is entirely under its Cu(I) form.

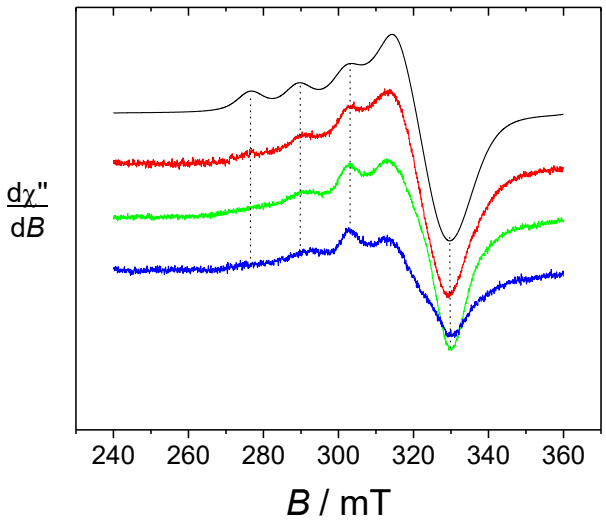

Fig 4. X-Band EPR spectra of 0.4 mM CH_3CN solutions of the *in situ* generated **1** (red), **2** (green), **3** (blue) and simulation by using the parameters given in the text (black). Spectra taken after 10 sec mixing at 293 K. Microwave Freq. 9.43 GHz, power 2.2 mW, Mod. Amp. 0.3 mT, Mod. Freq. 100 KHz.

UV-visible spectra of the complexes performed in DMF are in line with the EPR experiments, with the presence of an intense band at 455 nm and a large low-intensity band near 800 nm, indicatives of the presence of the Cu(I) form of the complex as the main product (Figure S5). This "auto-reduction" phenomenon have been already investigated in the case of 6,6'dialkyl-2,2 '-bipyridine ligand [65]. Partial and slow reduction have also been observed for the parent complex $Cu^{II}(dmp)_2$ without being further investigated.[66,67] In this work, the fast reduction of all three complexes, especially in DMF, is undoubtedly triggered by the high redox potential and the higher constraint brought by the bulky substituent to the Cu(II) geometry. This is especially the case in non-coordinating solvent, where the Cu(II) metal cannot coordinate a fifth ligand to adopt a more favorable geometry. Note that the exact nature of the reductant could not be identified.

Functionalization of MWCNTs with complexes 1,2 and 3

MWCNT electrodes were soaked in a 2 mmolL^{-1} MeCN solution of the corresponding complexes for 1 h. All bis(2,9-dialkyl-1,10-phenanthroline)copper(II) catalysts exhibit strong interactions with the MWCNT sidewalls owing to the pi-pi interactions at CNT sidewalls for the different polyaromatic bis(phenanthroline) complexes. XPS experiments were performed on MWCNT electrodes modified with complexes **1-3**. XPS spectra are similar for all complexes (Figure 5, Figure S6).

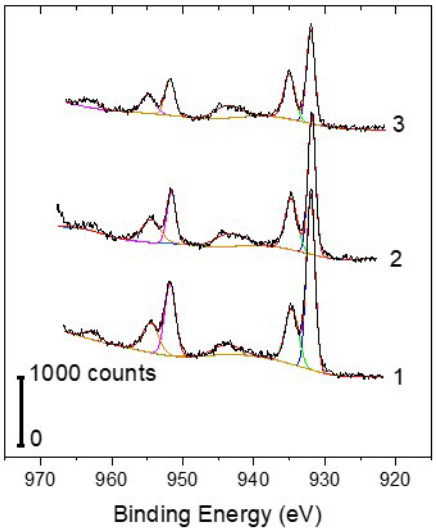

Figure 5. XPS spectra at Cu2p core energy level for the MWCNT electrodes modified with complexes **1, 2** and **3**

The presence of the Cu(II) form of the complexes is indicated by the peaks at 934.7 and 954.6 eV accompanied with satellite peaks at 944 and 963 eV. This is characteristic for adsorbed Cu(II) species. A second system with peaks at 931.9 and 951.7 eV can be assigned to the Cu(I) form of the complexes. According to the simulation of the XPS spectra and the integration of the peaks, the Cu(I) form is mainly present over Cu(II) form in a 70/30 ratio at the surface of the electrodes.

The presence of a majority of the Cu(I) species for all complexes is expected from the reduction of Cu(II) into Cu(I) under the XPS beam, which is often observed for copper complexes.[40,41,68] It is even more prevalent here since this series of complexes can be easily reduced, as observed by electrochemistry and EPR.

The electrochemical behavior of the functionalized MWCNT electrodes were investigated by cyclic voltammetry (CV) under argon and oxygen using a perchlorate buffer solution at pH 5 (Figure 6).

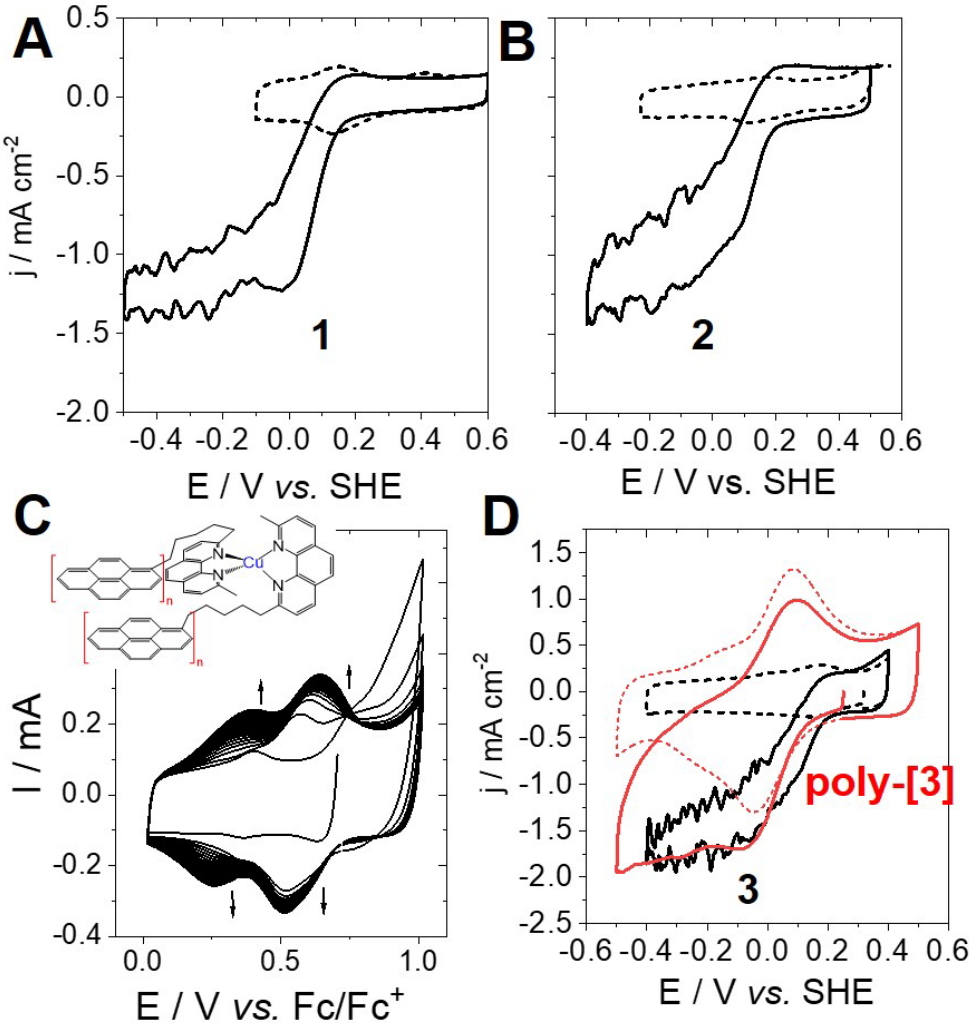

Figure 6. (A) CV of complex **1** and (B) complex **2** and **3** immobilized on a MWCNT electrode in a perchlorate buffer (100 mM NaClO4, 20 mM NaAcO, 20 mM AcOH) at pH 5 under (a) argon and (b) oxygen (v = 10 mV s^{-1}) ; (C) CVs of a solution of complex (C) **3** (20 scans between 0 and 1.0 V) at a MWCNT electrode in 0.1 M MeCN-TBAP (v = 100 mV s^{-1}) ; (D) CV of (black) complex **3** and (red) electropolymerized complex **3** on a MWCNT electrode in a perchlorate buffer (100 mM NaClO4, 20 mM NaAcO, 20 mM AcOH) at pH 5 under (a) argon and (b) oxygen (v = 10 mV s^{-1})

A reversible redox system is observed for all complexes in the perchlorate buffer. This redox system is assigned to the Cu^{II}/Cu^{I} redox couple. The ΔE for all complexes falls in the range 20 to 50 mV, which is expected from the surface-confined redox process. Complex **1**, **2** and **3** exhibit closed redox potentials, in line with the presence of bulky alkyl groups. In the case of complex 3, electropolymerisation of the complex was also performed at a MWCNT electrode (Figure 6C). During the course of the electropolymerisation, the increasing redox system observed at corresponds to the Cu(II)/Cu(I) reversible oxidation. The increasing redox system observed at corresponds to the electroactivity of the polypyrene backbone, which was already investigated at other types of electrogenerated polypyrene films.[49,55]

The integration of the charge under the reduction or the oxidation peak of the Cu(II)/ Cu(I) couple gives access to a surface coverage of 0.12, 0.062 and 0.17 nmol cm^{-2} for complexes **1**, **2** and **3** respectively. Comparing the immobilization of complex **1** and **2** with complex **3**, a minor improvement towards catalyst loadings is observed by adding pyrene groups. This likely arises from the strong interaction of all bis(2,9-dialkyl-1,10-phenanthroline)copper complexes with CNT sidewalls, taking into account the presence of pi-conjugated planar phenanthroline ligands

associated with bulky hydrophobic groups. On the contrary, electropolymerisation, associated with strong interaction between CNT sidewalls and the polypyrene backbone, gives access to high surface loadings of 2.2 nmol cm^{-2}.

When oxygen is purged into the electrochemical cell, an irreversible reduction wave is observed, occurring at closed redox potential for the series of complexes. Despite higher catalyst loading for complex 3 and its metallopolymer counterpart, no apparent increase in catalytic currents are observed for these functionalized electrodes. These similar current densities for all electrodes indicate the mass transport limitations of oxygen at this MWCNT electrodes.

ORR performances were investigated by RRDE (Figure 7, table 1).

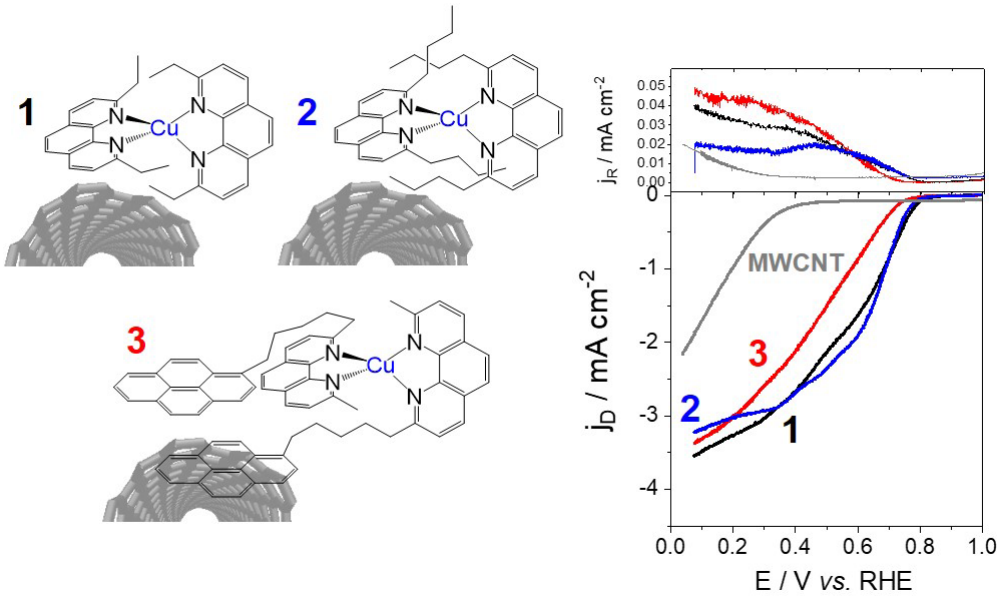

Figure 7. Plot of the disk current (J_D) *vs.* disk potential and plot of the ring current (J_R) vs disk potential for Rotating Ring Disk Electrode (RRDE) measurements performed under O_2 at the MWCNT electrode functionalized with complex **1, 2** and **3** using linear sweep voltammetry (10 mV s^{-1}, 1500 rpm, 100 mM $NaClO_4$, 20 mM NaAcO, 20 mM AcOH buffer pH = 5)

Table 1. Electrochemical parameters, ORR characteristics and fuel cell performances for complex **1**, **2** and **3**.

	$E_{p1/2}$ (V *vs.* RHE)	E_{onset} (V vs. RHE)	% H_2O_2	n electrons	Fuel cell OCV (V)	Fuel cell maximum power output (mW cm^{-2})
1	0.68	0.91	8 (+/-2)	3.9 (+/-0.2)	0.76 (+/-0.06)	1.77
2	0.68	0.90	4 (+/-2)	3.9 (+/-0.2)	0.85 (+/-0.08)	0.56
3	0.69	0.86	10 (+/-2)	3.8 (+/-0.2)	0.80 (+/-0.08)	1.10

According to current density measured at the Pt ring electrode, low amounts of H_2O_2 between 4 and 10 % are produced during ORR for all complexes at pH 5. Furthermore, a number of electrons of 3.8-3.9 were measured for all complexes. This confirms the ORR mechanism is closed to a 4H+/4e- mechanism. Furthermore, all complexes exhibit similar onset potentials, indicating that the different electronic contributions of alkyl groups in the 2 and 9 positions of the phenanthroline has a negligible effect on the redox potential of the catalytic intermediate in water. In this respect, the dinuclear nature of this intermediate have been postulated by different groups at supported mononuclear copper complexes based on phenanthroline or trispyridylmethyl-based ligands It is noteworthy that onset potential for complex **3** is slightly higher by 50 mV. This might arise from the steric hindrance brought by the pentylpyrene moiety, which might influence the redox potential of the ORR catalytic intermediate. Owing to the fact that efficient wiring of copper catalysts is obtained at these MWCNT electrodes as compared to EPG electrodes, the ORR is not limited by

the kinetics of the oxygen reduction. This allows the copper complexes bearing bulkier groups to achieve high electrocatalytic activity, contrary to what was observed at EPG electrodes.[56] In this previous work, monofunctionalized Cu^{II} complexes were formed by mixing different substituted phenanthroline ligands at the EPG electrode, their ORR being governed by the kinetic limitations of these derivatives. He we show that onset potentials of MWCNT-supported complexes are among the highest potential measured for copper complexes towards ORR near neutral pH. Other types of mononuclear or dinuclear complexes based on different trispyridylmethylamine [33,40,41] and triazol[36,43,44] ligands exhibit maximum onset potentials of 0.82 V vs. RHE at pH 7.

These complexes were finally integrated in a gas-diffusion H_2/air fuel cell (Figure 8A).

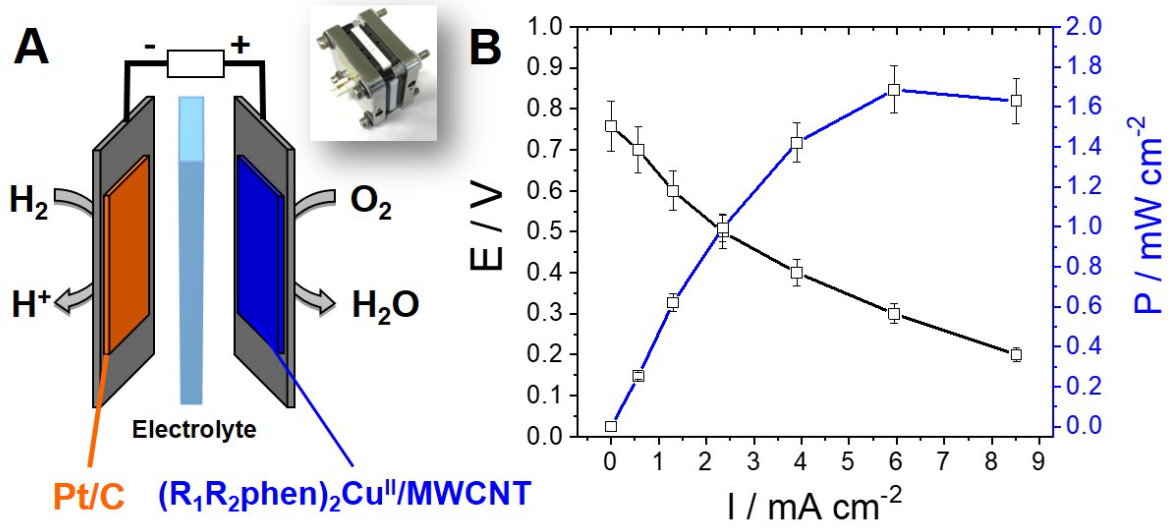

Figure 8. (A) Schematic representation and photograph of the H_2/air fuel cell; (B) Polarization and power curves for the fuel cell with a cathode based on a MWCNT-coated GDE modified with complex **1** (0.1 M Britton-Robinson buffer pH = 4, 25°C)

First, the complexes were immobilized on a MWCNT-coated gas-diffusion electrode (GDE). A conventional Pt/C catalyst (1 mg cm^{-2}) was used at the anode. Fig. 8A shows the schematic representation of the H_2/air fuel cell set-up. Both electrodes were separated by a 5 mm thick teflon chamber in which a pH 4 buffer electrolyte was introduced. While the fuel cell was operated at 25°C, the electrodes were both supplied with humidified streams of H_2 and air respectively at atmospheric pressure. The polarization and power curves were obtained from successive galvanostatic discharges (Figure 8B, Figure S7). The H_2/air fuel cells deliver maximum power density of 1.77, 0.56 and 1.10 mW cm^{-2} for complex **1**, **2** and **3** respectively, accompanied with respective open-circuit voltage (OCV) of 0.76, 0.85 and 0.84 V. These fuel cells based on this series of MWCNT-supported bis(2,9-dialkyl-1,10-phenanthroline)copper complexes as cathodic material exhibit unprecedented fuel cell performances at low pH. These fuel cells approach the

performances of enzymatic fuel cells based on hydrogenases and multicopper oxidases which exhibit maximum power output of several mW cm^{-2} accompanied with high OCV of 1.1 V.[69,70] Furthermore, these fuel cells outperform previously-designed H_2/air fuel cells integrating molecular catalysts, which have all be limited by the performances of the ORR catalysts at the cathode. Ni-Ru catalysts integrated in H_2/air fuel cells deliver maximum power output of 26 μW cm^{-2} with an OCV of 0.42 V.[71,72] We recently designed H_2/air fuel cells based on bioinspired nickel bis-diphosphine catalysts at the anode. These fuel cells delivered 2 mW cm^{-2} with an OCV of 1 V by using a MWCNT-supported multicopper enzyme at the cathode.[26] More recently, a bioinspired dinuclear copper catalyst at the cathode was combined to the same bioinspired nickel catalyst at the anode. This fuel cell delivered 0.15 mW cm^{-2} at pH 4 accompanied with an OCV of 0.6 V.[40]

In summary we report the functionalization of MWCNTs with a series of bis(2,9-dialkyl-1,10-phenanthroline)copper complexes. Owing to the presence of bulky groups at the 2 and 9 position of the phen ligands, these complexes exhibit distorted square-planar geometry, high Cu(II)/Cu(I) redox potential, and strong interactions with CNT sidewalls. The bis(2,9-diethyl-1,10-phenanthroline)copper catalysts possess the best combination of redox potential and interactions with MWCNT electrodes. These MWCNT-supported catalysts exhibit high potential towards ORR with unprecedented onset potentials of 0.91 V vs. RHE at pH 5. Despite the fact that onset potentials are still lower as compared to onset potentials of MWCNT-supported laccases (onset potentials of 1.1 V vs. RHE at pH 5[73]), these complexes were integrated in a MWCNT-GDE H_2/air fuel cell exhibiting OCV of 0.8 V and maximum power output of 1.77 mW cm-2. This series of MWCNT-supported catalysts pave the way in the approach of both multicopper enzymes and Pt performances towards low-pH ORR for proton-exchange membrane fuel cells. Future developments will be aimed at tuning the geometry of copper centers in multinuclear complexes

in order to approach the structure and performances of copper enzymes where a set of four copper centres in a semi-rigid environment is responsible for their low-overpotential ORR requirement.

Supporting Information. Experimental details, Table S1 and Figure S1 to S7

Corresponding Author

Alan.le-goff@univ-grenoble-alpes.fr

Author Contributions

The manuscript was written with contributions of all authors. All authors have given approval to the final version of the manuscript.

Acknowledgments

This work was supported by the Ministère de l'Environnement, de l'Energie et de la Mer and the Agence Nationale de la Recherche through the LabEx ARCANE programe (ANR-11-LABX-0003-01), the Graduate School on Chemistry, Biology and Health of Univ Grenoble Alpes CBH-EUR-GS (ANR-17-EURE-0003) and the ANR project BioNics (ANR-17-CE09-0013). The authors acknowledge support from the plateforme de Chimie NanoBio ICMG FR 2607 (PCN-ICMG) and Plateau Synthese Organique (PSO-DCM). Valérie Flaud and Dominique Granier from

Institut Charles Gerhardt (University of Montpellier 2) are gratefully acknowledged for XPS analysis.

REFERENCES

(1) Shao, M.; Chang, Q.; Dodelet, J.-P.; Chenitz, R. Recent Advances in Electrocatalysts for Oxygen Reduction Reaction. *Chem. Rev.* **2016**, *116* (6), 3594–3657. https://doi.org/10.1021/acs.chemrev.5b00462.

(2) Jaouen, F.; Proietti, E.; Lefèvre, M.; Chenitz, R.; Dodelet, J.-P.; Wu, G.; Chung, H. T.; Johnston, C. M.; Zelenay, P. Recent Advances in Non-Precious Metal Catalysis for Oxygen-Reduction Reaction in Polymer Electrolyte Fuel Cells. *Energy Environ. Sci.* **2010**, *4* (1), 114–130. https://doi.org/10.1039/C0EE00011F.

(3) Pegis, M. L.; Wise, C. F.; Martin, D. J.; Mayer, J. M. Oxygen Reduction by Homogeneous Molecular Catalysts and Electrocatalysts. *Chem. Rev.* **2018**, *118* (5), 2340–2391. https://doi.org/10.1021/acs.chemrev.7b00542.

(4) Soukharev, V.; Mano, N.; Heller, A. A Four-Electron O2-Electroreduction Biocatalyst Superior to Platinum and a Biofuel Cell Operating at 0.88 V. *J. Am. Chem. Soc.* **2004**, *126* (27), 8368–8369. https://doi.org/10.1021/ja0475510.

(5) Blanford, C. F.; Heath, R. S.; Armstrong, F. A. A Stable Electrode for High-Potential, Electrocatalytic O2 Reduction Based on Rational Attachment of a Blue Copper Oxidase to a Graphite Surface. *Chem. Commun.* **2007**, 1710–1712. https://doi.org/10.1039/B703114A.

(6) Le Goff, A.; Holzinger, M.; Cosnier, S. Recent Progress in Oxygen-Reducing Laccase Biocathodes for Enzymatic Biofuel Cells. *Cell. Mol. Life Sci.* **2015**, *72* (5), 941–952. https://doi.org/10.1007/s00018-014-1828-4.

(7) Chen, H.; Simoska, O.; Lim, K.; Grattieri, M.; Yuan, M.; Dong, F.; Lee, Y. S.; Beaver, K.; Weliwatte, S.; Gaffney, E. M.; Minteer, S. D. Fundamentals, Applications, and Future Directions of Bioelectrocatalysis. *Chem. Rev.* **2020**, *120* (23), 12903–12993. https://doi.org/10.1021/acs.chemrev.0c00472.

(8) Lewis, E. A.; Tolman, W. B. Reactivity of Dioxygen−Copper Systems. *Chem. Rev.* **2004**, *104* (2), 1047–1076. https://doi.org/10.1021/cr020633r.

(9) Solomon, E. I.; Heppner, D. E.; Johnston, E. M.; Ginsbach, J. W.; Cirera, J.; Qayyum, M.; Kieber-Emmons, M. T.; Kjaergaard, C. H.; Hadt, R. G.; Tian, L. Copper Active Sites in Biology. *Chem. Rev.* **2014**, *114* (7), 3659–3853. https://doi.org/10.1021/cr400327t.

(10) Whittaker, J. W. Free Radical Catalysis by Galactose Oxidase. *Chem. Rev.* **2003**, *103* (6), 2347–2364. https://doi.org/10.1021/cr020425z.

(11) Mano, N.; de Poulpiquet, A. O2 Reduction in Enzymatic Biofuel Cells. *Chem. Rev.* **2017**, *118* (5), 2392–2468. https://doi.org/10.1021/acs.chemrev.7b00220.

(12) Bullock, R. M.; Chen, J. G.; Gagliardi, L.; Chirik, P. J.; Farha, O. K.; Hendon, C. H.; Jones, C. W.; Keith, J. A.; Klosin, J.; Minteer, S. D.; Morris, R. H.; Radosevich, A. T.; Rauchfuss, T. B.; Strotman, N. A.; Vojvodic, A.; Ward, T. R.; Yang, J. Y.; Surendranath, Y. Using Nature's Blueprint to Expand Catalysis with Earth-Abundant Metals. *Science* **2020**, *369* (6505). https://doi.org/10.1126/science.abc3183.

(13) Fukuzumi, S.; Lee, Y.-M.; Nam, W. Mechanisms of Two-Electron versus Four-Electron Reduction of Dioxygen Catalyzed by Earth-Abundant Metal Complexes. *ChemCatChem* **2018**, *10* (1), 9–28. https://doi.org/10.1002/cctc.201701064.
(14) Zhao, Y.-M.; Yu, G.-Q.; Wang, F.-F.; Wei, P.-J.; Liu, J.-G. Bioinspired Transition-Metal Complexes as Electrocatalysts for the Oxygen Reduction Reaction. *Chemistry – A European Journal* **2019**, *25* (15), 3726–3739. https://doi.org/10.1002/chem.201803764.
(15) Bullock, R. M.; Das, A. K.; Appel, A. M. Surface Immobilization of Molecular Electrocatalysts for Energy Conversion. *Chemistry – A European Journal* **2017**, *23* (32), 7626–7641. https://doi.org/10.1002/chem.201605066.
(16) Thorseth, M. A.; Tornow, C. E.; Tse, E. C. M.; Gewirth, A. A. Cu Complexes That Catalyze the Oxygen Reduction Reaction. *Coordination Chemistry Reviews* **2013**, *257* (1), 130–139. https://doi.org/10.1016/j.ccr.2012.03.033.
(17) Mangue, J.; Gondre, C.; Pécaut, J.; Duboc, C.; Ménage, S.; Torelli, S. Controlled O2 Reduction at a Mixed-Valent (II,I) Cu2S Core. *Chem. Commun.* **2020**, *56* (67), 9636–9639. https://doi.org/10.1039/D0CC03987J.
(18) Itoh, S. Developing Mononuclear Copper–Active-Oxygen Complexes Relevant to Reactive Intermediates of Biological Oxidation Reactions. *Acc. Chem. Res.* **2015**, *48* (7), 2066–2074. https://doi.org/10.1021/acs.accounts.5b00140.
(19) Machan, C. W. Advances in the Molecular Catalysis of Dioxygen Reduction. *ACS Catal.* **2020**, *10* (4), 2640–2655. https://doi.org/10.1021/acscatal.9b04477.
(20) Hong, S.; Lee, Y.-M.; Ray, K.; Nam, W. Dioxygen Activation Chemistry by Synthetic Mononuclear Nonheme Iron, Copper and Chromium Complexes. *Coordination Chemistry Reviews* **2017**, *334*, 25–42. https://doi.org/10.1016/j.ccr.2016.07.006.
(21) Kakuda, S.; Peterson, R. L.; Ohkubo, K.; Karlin, K. D.; Fukuzumi, S. Enhanced Catalytic Four-Electron Dioxygen (O2) and Two-Electron Hydrogen Peroxide (H2O2) Reduction with a Copper(II) Complex Possessing a Pendant Ligand Pivalamido Group. *J. Am. Chem. Soc.* **2013**, *135* (17), 6513–6522. https://doi.org/10.1021/ja3125977.
(22) Smits, N. W. G.; van Dijk, B.; de Bruin, I.; Groeneveld, S. L. T.; Siegler, M. A.; Hetterscheid, D. G. H. Influence of Ligand Denticity and Flexibility on the Molecular Copper Mediated Oxygen Reduction Reaction. *Inorg. Chem.* **2020**, *59* (22), 16398–16409. https://doi.org/10.1021/acs.inorgchem.0c02204.
(23) Artero, V. Bioinspired Catalytic Materials for Energy-Relevant Conversions. *Nat. Energy* **2017**, *2* (9), 17131. https://doi.org/10.1038/nenergy.2017.131.
(24) Dey, S.; Mondal, B.; Chatterjee, S.; Rana, A.; Amanullah, S. K.; Dey, A. Molecular Electrocatalysts for the Oxygen Reduction Reaction. *Nat. Rev. Chem.* **2017**, *1* (12), UNSP 0098. https://doi.org/10.1038/s41570-017-0098.
(25) Coutard, N.; Reuillard, B.; Huan, T. N.; Valentino, F.; Jane, R. T.; Gentil, S.; Andreiadis, E.; Le Goff, A.; Asset, T.; Maillard, F.; Jousselme, B.; Morozan, A.; Lyonnard, S.; Artero, V.; Chenevier, P. Impact of Ionomer Structuration on the Performance of Bio-Inspired Noble-Metal-Free Fuel Cell Anodes. *Chem Catalysis* **2021**. https://doi.org/10.1016/j.checat.2021.01.001.
(26) Gentil, S.; Lalaoui, N.; Dutta, A.; Nedellec, Y.; Cosnier, S.; Shaw, W. J.; Artero, V.; Le Goff, A. Carbon-Nanotube-Supported Bio-Inspired Nickel Catalyst and Its Integration in Hybrid Hydrogen/Air Fuel Cells. *Angew. Chem. Int. Ed.* **2017**, *56* (7), 1845–1849. https://doi.org/10.1002/anie.201611532.

(27) Huan, T. N.; Jane, R. T.; Benayad, A.; Guetaz, L.; Tran, P. D.; Artero, V. Bio-Inspired Noble Metal-Free Nanomaterials Approaching Platinum Performances for H2 Evolution and Uptake. *Energy Environ. Sci.* **2016**, *9* (3), 940–947. https://doi.org/10.1039/C5EE02739J.
(28) Le Goff, A.; Artero, V.; Jousselme, B.; Tran, P. D.; Guillet, N.; Metaye, R.; Fihri, A.; Palacin, S.; Fontecave, M. From Hydrogenases to Noble Metal-Free Catalytic Nanomaterials for H2 Production and Uptake. *Science* **2009**, *326* (5958), 1384–1387.
(29) Wilson, A. D.; Newell, R. H.; McNevin, M. J.; Muckerman, J. T.; Rakowski DuBois, M.; DuBois, D. L. Hydrogen Oxidation and Production Using Nickel-Based Molecular Catalysts with Positioned Proton Relays. *J. Am. Chem. Soc.* **2006**, *128* (1), 358–366. https://doi.org/10.1021/ja056442y.
(30) Dutta, A.; Roberts, J. A. S.; Shaw, W. J. Arginine-Containing Ligands Enhance H2 Oxidation Catalyst Performance. *Angew. Chem. Int. Ed.* **2014**, *53* (25), 6487–6491. https://doi.org/10.1002/anie.201402304.
(31) Chen, Z.; Higgins, D.; Yu, A.; Zhang, L.; Zhang, J. A Review on Non-Precious Metal Electrocatalysts for PEM Fuel Cells. *Energy & Environmental Science* **2011**, *4* (9), 3167–3192. https://doi.org/10.1039/C0EE00558D.
(32) Gewirth, A. A.; Varnell, J. A.; DiAscro, A. M. Nonprecious Metal Catalysts for Oxygen Reduction in Heterogeneous Aqueous Systems. *Chem. Rev.* **2018**, *118* (5), 2313–2339. https://doi.org/10.1021/acs.chemrev.7b00335.
(33) Thorseth, M. A.; Letko, C. S.; Rauchfuss, T. B.; Gewirth, A. A. Dioxygen and Hydrogen Peroxide Reduction with Hemocyanin Model Complexes. *Inorg. Chem.* **2011**, *50* (13), 6158–6162. https://doi.org/10.1021/ic200386d.
(34) Thorseth, M. A.; Letko, C. S.; Tse, E. C. M.; Rauchfuss, T. B.; Gewirth, A. A. Ligand Effects on the Overpotential for Dioxygen Reduction by Tris(2-Pyridylmethyl)Amine Derivatives. *Inorg. Chem.* **2013**, *52* (2), 628–634. https://doi.org/10.1021/ic301656x.
(35) Slowiński, K.; Kublik, Z.; Bilewicz, R.; Pietraszkiewicz, M. Electrocatalysis of Oxygen Reduction by a Copper(II) Hexaazamacrocyclic Complex. *J. Chem. Soc., Chem. Commun.* **1994**, No. 9, 1087–1088. https://doi.org/10.1039/C39940001087.
(36) Thorum, M. S.; Yadav, J.; Gewirth, A. A. Oxygen Reduction Activity of a Copper Complex of 3,5-Diamino-1,2,4-Triazole Supported on Carbon Black. *Angew. Chem. Int. Ed.* **2009**, *48* (1), 165–167. https://doi.org/10.1002/anie.200803554.
(37) Brushett, F. R.; Thorum, M. S.; Lioutas, N. S.; Naughton, M. S.; Tornow, C.; Jhong, H.-R. "Molly"; Gewirth, A. A.; Kenis, P. J. A. A Carbon-Supported Copper Complex of 3,5-Diamino-1,2,4-Triazole as a Cathode Catalyst for Alkaline Fuel Cell Applications. *J. Am. Chem. Soc.* **2010**, *132* (35), 12185–12187. https://doi.org/10.1021/ja104767w.
(38) Wang, F.-F.; Zhao, Y.-M.; Wei, P.-J.; Zhang, Q.-L.; Liu, J.-G. Efficient Electrocatalytic O2 Reduction at Copper Complexes Grafted onto Polyvinylimidazole Coated Carbon Nanotubes. *Chem. Commun.* **2017**, *53* (9), 1514–1517. https://doi.org/10.1039/C6CC08552K.
(39) Gentil, S.; Serre, D.; Philouze, C.; Holzinger, M.; Thomas, F.; Le Goff, A. Electrocatalytic O2 Reduction at a Bio-Inspired Mononuclear Copper Phenolato Complex Immobilized on a Carbon Nanotube Electrode. *Angew. Chem. Int. Ed.* **2016**, *55* (7), 2517–2520. https://doi.org/10.1002/anie.201509593.
(40) Gentil, S.; Molloy, J. K.; Carrière, M.; Hobballah, A.; Dutta, A.; Cosnier, S.; Shaw, W. J.; Gellon, G.; Belle, C.; Artero, V.; Thomas, F.; Le Goff, A. A Nanotube-Supported Dicopper

Complex Enhances Pt-Free Molecular H2/Air Fuel Cells. *Joule* **2019**, *3* (8), 2020–2029. https://doi.org/10.1016/j.joule.2019.07.001.

(41) Gentil, S.; Molloy, J. K.; Carrière, M.; Gellon, G.; Philouze, C.; Serre, D.; Thomas, F.; Le Goff, A. Substituent Effects in Carbon-Nanotube-Supported Copper Phenolato Complexes for Oxygen Reduction Reaction. *Inorg. Chem.* **2021**, *60* (10), 6922–6929. https://doi.org/10.1021/acs.inorgchem.1c00157.

(42) Xi, Y.-T.; Wei, P.-J.; Wang, R.-C.; Liu, J.-G. Bio-Inspired Multinuclear Copper Complexes Covalently Immobilized on Reduced Graphene Oxide as Efficient Electrocatalysts for the Oxygen Reduction Reaction. *Chem. Commun.* **2015**, *51* (35), 7455–7458. https://doi.org/10.1039/C5CC00963D.

(43) Kato, M.; Muto, M.; Matsubara, N.; Uemura, Y.; Wakisaka, Y.; Yoneuchi, T.; Matsumura, D.; Ishihara, T.; Tokushima, T.; Noro, S.; Takakusagi, S.; Asakura, K.; Yagi, I. Incorporation of Multinuclear Copper Active Sites into Nitrogen-Doped Graphene for Electrochemical Oxygen Reduction. *ACS Appl. Energy Mater.* **2018**, *1* (5), 2358–2364. https://doi.org/10.1021/acsaem.8b00491.

(44) Iwase, K.; Yoshioka, T.; Nakanishi, S.; Hashimoto, K.; Kamiya, K. Copper-Modified Covalent Triazine Frameworks as Non-Noble-Metal Electrocatalysts for Oxygen Reduction. *Angewandte Chemie International Edition* **2015**, *54* (38), 11068–11072. https://doi.org/10.1002/anie.201503637.

(45) Hijazi, I.; Bourgeteau, T.; Cornut, R.; Morozan, A.; Filoramo, A.; Leroy, J.; Derycke, V.; Jousselme, B.; Campidelli, S. Carbon Nanotube-Templated Synthesis of Covalent Porphyrin Network for Oxygen Reduction Reaction. *J. Am. Chem. Soc.* **2014**, *136* (17), 6348–6354. https://doi.org/10.1021/ja500984k.

(46) Morozan, A.; Campidelli, S.; Filoramo, A.; Jousselme, B.; Palacin, S. Catalytic Activity of Cobalt and Iron Phthalocyanines or Porphyrins Supported on Different Carbon Nanotubes towards Oxygen Reduction Reaction. *Carbon* **2011**, *49* (14), 4839–4847. https://doi.org/10.1016/j.carbon.2011.07.004.

(47) Le Goff, A.; Gorgy, K.; Holzinger, M.; Haddad, R.; Zimmerman, M.; Cosnier, S. Tris(Bispyrene-bipyridine)Iron(II): A Supramolecular Bridge for the Biofunctionalization of Carbon Nanotubes via Π-Stacking and Pyrene/B-Cyclodextrin Host–Guest Interactions. *Chem. Eur. J.* **2011**, *17* (37), 10216–10221.

(48) Reuillard, B.; Le Goff, A.; Holzinger, M.; Serge Cosnier. Non-Covalent Functionalization of Carbon Nanotubes with Boronic Acids for the Wiring of Glycosylated Redox Enzymes in Oxygen-Reducing Biocathodes. *J. Mater. Chem. B* **2014**, *2* (16), 2228–2232. https://doi.org/10.1039/C3TB21846E.

(49) Le Goff, A.; Reuillard, B.; Cosnier, S. A Pyrene-Substituted Tris(Bipyridine)Osmium(II) Complex as a Versatile Redox Probe for Characterizing and Functionalizing Carbon Nanotube- and Graphene-Based Electrodes. *Langmuir* **2013**, *29* (27), 8736–8742. https://doi.org/10.1021/la401712u.

(50) Rajabi, S.; Ebrahimi, F.; Lole, G.; Odrobina, J.; Dechert, S.; Jooss, C.; Meyer, F. Water Oxidizing Diruthenium Electrocatalysts Immobilized on Carbon Nanotubes: Effects of the Number and Positioning of Pyrene Anchors. *ACS Catal.* **2020**, *10* (18), 10614–10626. https://doi.org/10.1021/acscatal.0c01577.

(51) Reuillard, B.; Ly, K. H.; Rosser, T. E.; Kuehnel, M. F.; Zebger, I.; Reisner, E. Tuning Product Selectivity for Aqueous CO2 Reduction with a Mn(Bipyridine)-Pyrene Catalyst

Immobilized on a Carbon Nanotube Electrode. *J. Am. Chem. Soc.* **2017**, *139* (41), 14425–14435. https://doi.org/10.1021/jacs.7b06269.

(52) Pugliese, S.; Huan, N. T.; Forte, J.; Grammatico, D.; Zanna, S.; Su, B.-L.; Li, Y.; Fontecave, M. Functionalization of Carbon Nanotubes with Nickel Cyclam for the Electrochemical Reduction of CO2. *ChemSusChem* **2020**, *13* (23), 6449–6456. https://doi.org/10.1002/cssc.202002092.

(53) Tran, P. D.; Le Goff, A.; Heidkamp, J.; Jousselme, B.; Guillet, N.; Palacin, S.; Dau, H.; Fontecave, M.; Artero, V. Noncovalent Modification of Carbon Nanotubes with Pyrene-Functionalized Nickel Complexes: Carbon Monoxide Tolerant Catalysts for Hydrogen Evolution and Uptake. *Angew. Chem.-Int. Edit.* **2011**, *50* (6), 1371–1374.

(54) Le Goff, A.; Moggia, F.; Debou, N.; Jegou, P.; Artero, V.; Fontecave, M.; Jousselme, B.; Palacin, S. Facile and Tunable Functionalization of Carbon Nanotube Electrodes with Ferrocene by Covalent Coupling and π-Stacking Interactions and Their Relevance to Glucose Bio-Sensing. *J. Electro. Anal. Chem.* **2010**, *641* (1–2), 57–63. https://doi.org/10.1016/j.jelechem.2010.01.014.

(55) Lalaoui, N.; Reuillard, B.; Philouze, C.; Holzinger, M.; Cosnier, S.; Le Goff, A. Osmium(II) Complexes Bearing Chelating N-Heterocyclic Carbene and Pyrene-Modified Ligands: Surface Electrochemistry and Electron Transfer Mediation of Oxygen Reduction by Multicopper Enzymes. *Organometallics* **2016**, *35* (17), 2987–2992. https://doi.org/10.1021/acs.organomet.6b00508.

(56) McCrory, C. C. L.; Ottenwaelder, X.; Stack, T. D. P.; Chidsey, C. E. D. Kinetic and Mechanistic Studies of the Electrocatalytic Reduction of O2 to H2O with Mononuclear Cu Complexes of Substituted 1,10-Phenanthrolines. *Journal of Physical Chemistry A* **2007**, *111* (49), 12641–12650.

(57) Venegas, R.; Muñoz-Becerra, K.; Lemus, L.; Toro-Labbé, A.; Zagal, J. H.; Recio, F. J. Theoretical and Experimental Reactivity Predictors for the Electrocatalytic Activity of Copper Phenanthroline Derivatives for the Reduction of Dioxygen. *J. Phys. Chem. C* **2019**, *123* (32), 19468–19478. https://doi.org/10.1021/acs.jpcc.9b03200.

(58) James, B. R.; Williams, R. J. P. 383. The Oxidation–Reduction Potentials of Some Copper Complexes. *J. Chem. Soc.* **1961**, *0* (0), 2007–2019. https://doi.org/10.1039/JR9610002007.

(59) Cunningham, C. T.; Moore, J. J.; Cunningham, K. L. H.; Fanwick, P. E.; McMillin, D. R. Structural and Photophysical Studies of Cu(NN)2+ Systems in the Solid State. Emission at Last from Complexes with Simple 1,10-Phenanthroline Ligands. *Inorg. Chem.* **2000**, *39* (16), 3638–3644. https://doi.org/10.1021/ic000082s.

(60) Leandri, V.; Daniel, Q.; Chen, H.; Sun, L.; Gardner, J. M.; Kloo, L. Electronic and Structural Effects of Inner Sphere Coordination of Chloride to a Homoleptic Copper(II) Diimine Complex. *Inorg. Chem.* **2018**, *57* (8), 4556–4562. https://doi.org/10.1021/acs.inorgchem.8b00225.

(61) Itoh, S.; Kishikawa, N.; Suzuki, T.; Takagi, H. D. Syntheses, Structural Analyses and Redox Kinetics of Four-Coordinate [CuL2]2+ and Five-Coordinate [CuL2(Solvent)]2+ Complexes (L = 6,6′-Dimethyl-2,2′-Bipyridine or 2,9-Dimethyl-1,10-Phenanthroline): Completely Gated Reduction Reaction of [Cu(Dmp)2]2+ in Nitromethane. *Dalton Trans.* **2005**, No. 6, 1066–1078. https://doi.org/10.1039/B415057K.

(62) Higashino, T.; Iiyama, H.; Nimura, S.; Kurumisawa, Y.; Imahori, H. Effect of Ligand Structures of Copper Redox Shuttles on Photovoltaic Performance of Dye-Sensitized Solar Cells. *Inorg. Chem.* **2020**, *59* (1), 452–459. https://doi.org/10.1021/acs.inorgchem.9b02740.

(63) Kovalevsky, A. Yu.; Gembicky, M.; Novozhilova, I. V.; Coppens, P. Solid-State Structure Dependence of the Molecular Distortion and Spectroscopic Properties of the Cu(I) Bis(2,9-Dimethyl-1,10-Phenanthroline) Ion. *Inorg. Chem.* **2003**, *42* (26), 8794–8802. https://doi.org/10.1021/ic0348805.
(64) Eggleston, M. K.; McMillin, D. R.; Koenig, K. S.; Pallenberg, A. J. Steric Effects in the Ground and Excited States of Cu(NN)2+ Systems. *Inorg. Chem.* **1997**, *36* (2), 172–176. https://doi.org/10.1021/ic960698a.
(65) Kitagawa, S.; Munakata, M.; Higashie, A. Autoreduction of Copper(II) Complexes of 6,6′-Diakyl-2,2′-Bipyridine and Characterization of Their Copper(I) Complexes. *Inorganica Chimica Acta* **1984**, *84* (1), 79–84. https://doi.org/10.1016/S0020-1693(00)87672-0.
(66) Levín, P.; C. Ruiz, M.; B. Romo, A. I.; R. Nascimento, O.; Virgilio, A. L. D.; G. Oliver, A.; P. Ayala, A.; N. Diógenes, I. C.; E. León, I.; Lemus, L. Water-Mediated Reduction of [Cu(Dmp) 2 (CH 3 CN)] 2+ : Implications of the Structure of a Classical Complex on Its Activity as an Anticancer Drug. *Inorganic Chemistry Frontiers* **2021**, *8* (13), 3238–3252. https://doi.org/10.1039/D1QI00233C.
(67) Doine, H.; Yano, Y.; Swaddle, T. W. *Kinetics of the bis(2,9-dimethyl-1,10-phenanthroline)copper(I/II) self exchange reaction in solution*. ACS Publications. https://pubs-acs-org.gaelnomade-2.grenet.fr/doi/abs/10.1021/ic00311a015 (accessed 2022-02-24). https://doi.org/10.1021/ic00311a015.
(68) Losev, A.; Rostov, K.; Tyuliev, G. Electron Beam Induced Reduction of CuO in the Presence of a Surface Carbonaceous Layer: An XPS/HREELS Study. *Surface Science* **1989**, *213* (2), 564–579. https://doi.org/10.1016/0039-6028(89)90313-0.
(69) Xia, H.; So, K.; Kitazumi, Y.; Shirai, O.; Nishikawa, K.; Higuchi, Y.; Kano, K. Dual Gas-Diffusion Membrane- and Mediatorless Dihydrogen/Air-Breathing Biofuel Cell Operating at Room Temperature. *Journal of Power Sources* **2016**, *335* (Supplement C), 105–112. https://doi.org/10.1016/j.jpowsour.2016.10.030.
(70) Gentil, S.; Che Mansor, S. M.; Jamet, H.; Cosnier, S.; Cavazza, C.; Le Goff, A. Oriented Immobilization of [NiFeSe] Hydrogenases on Covalently and Noncovalently Functionalized Carbon Nanotubes for H2/Air Enzymatic Fuel Cells. *ACS Catal.* **2018**, 3957–3964. https://doi.org/10.1021/acscatal.8b00708.
(71) Matsumoto, T.; Kim, K.; Ogo, S. Molecular Catalysis in a Fuel Cell. *Angew. Chem. Int. Ed.* **2011**, *50* (47), 11202–11205. https://doi.org/10.1002/anie.201104498.
(72) Matsumoto, T.; Kim, K.; Nakai, H.; Hibino, T.; Ogo, S. Organometallic Catalysts for Use in a Fuel Cell. *ChemCatChem* **2013**, *5* (6), 1368–1373. https://doi.org/10.1002/cctc.201200595.
(73) Lalaoui, N.; David, R.; Jamet, H.; Holzinger, M.; Le Goff, A.; Cosnier, S. Hosting Adamantane in the Substrate Pocket of Laccase: Direct Bioelectrocatalytic Reduction of O2 on Functionalized Carbon Nanotubes. *ACS Catal.* **2016**, *6*, 4259–4264. https://doi.org/10.1021/acscatal.6b00797.